High-resolution photoemission study of the low-energy excitations in 4f-electron systems

F. Patthey,* J.-M. Imer, W.-D. Schneider,* H. Beck, and Y. Baer
Institut de Physique, Université de Neuchâtel, CH-2000, Switzerland

B. Delley
Paul Scherrer Institut, Badenerstrasse 569, CH-8048 Zürich, Switzerland
(Received 14 May 1990)

We present an extensive photoemission study of the low-energy excitations in a series of Ce and Yb systems showing quite different electronic properties resulting from the weak hybridization of the 4f electrons with band states. We discuss briefly the application of the single-impurity model to the calculation of the excitation spectra and review the influence of the different parameters. We analyze the spectra of each compound separately and show that they can be remarkably well simulated within the single-impurity framework. From these data we attempt to predict the linear coefficient of the specific heat and the magnetic susceptibility at $T=0$ K. A comparison with experimental values points to the limitations of this model to yield a unified description of different properties.

I. INTRODUCTION

One of the fundamental motivations for electron-spectroscopic studies of solids is to deduce their electronic properties from their excitation spectra. Among the high-energy spectroscopies, photoemission has become very popular because it is commonly considered as one of the most direct methods to probe the density of the electronic states (DOS) in solids. The validity of this assumption is based on the Koopman approximation.[1] It states that, for deep core levels or valence-band states belonging to broad bands, the single-electron eigenvalues obtained from a mean-field calculation are nearly identical with the binding energies required to remove the considered electrons from the solid. However, when the correlation among the band electrons increases, the relationship between measured spectra and DOS is no longer straightforward.[2] This situation occurs for electrons belonging to a partly filled shell with a large orbital quantum number like 3d, 4f, and 5f. Among those the 4f states form rather well-localized charges, whereas their binding energies are of the order of the usual bandwidth. Consequently these states tend to hybridize with the band states and to contribute weakly to cohesion. In such systems the single-particle picture fails to account for many properties involving their excitations. In particular, at low temperatures, the quasiequilibrium methods (specific heat, susceptibility, transport properties) applied to the study of systems containing lanthanides, reveal very unusual manifestations characterized by the term "heavy-fermion behavior."[3,4]

The single-impurity model of Anderson, allowing the mixing of one localized 4f state with extended states, has proven to yield a first approach to many important aspects of this problem.[4] In particular, it has been used to calculate the spectral functions of high-energy spectroscopies.[5-7] The comparison with experiments, performed with a resolution of about two orders of magnitude larger than the characteristic energy scale of these many-body manifestations, has demonstrated that this model contains the essential mechanisms allowing one to account for the observed excitations.[8-14] In this way the parameters defined in the Anderson model can be determined and, within the same model, the low-energy thermodynamic properties can be estimated.[15] However, it is an experimental challenge to observe directly the low-lying many-body excitations close to the ground state and responsible for the unconventional low-temperature properties of hybridized f systems. Unfortunately, with the commonly achieved experimental resolution this goal remained unrealistic for a long time. We have shown recently[16-25] that with a resolution improvement of a factor of 10 (<20 meV) these narrow bands of low-lying excitations are accessible to experiment. These high-resolution photoemission results reveal interesting aspects when they are linked to those obtained by low-energy methods.

The aim of the present paper is to review the high-resolution results and their analysis in a systematic way in order to illustrate that at this energy scale these techniques open new possibilities to investigate the properties of condensed matter. The paper is organized as follows. In Sec. II, basic considerations on the single-impurity model applied to electron spectroscopies and the model calculation are briefly reviewed. The excitation spectra and their dependance on the different parameters are described qualitatively in Sec. III. Details on the instrument and the sample preparation are given in Sec. IV. The spectra of seven rare-earth systems and their analysis are presented in Sec. V. Finally in Sec. VI, a unified interpretation of all these data is performed and an attempt is made to compare them with the results obtained by low-energy techniques.

II. THE SINGLE-IMPURITY MODEL

A. General considerations

All experimental data presented and discussed in this paper will be interpreted theoretically on the basis of the

single-impurity model. The latter has proven to be very useful, in particular, for photoemission spectra, even though coherence effects due to the lattice are neglected. The starting point is the following Hamiltonian:

$$H=\sum_{\mathbf{k}\sigma}\varepsilon_{\mathbf{k}}c^{\dagger}_{\mathbf{k}\sigma}c_{\mathbf{k}\sigma}+\sum_{m\sigma}\varepsilon_f a^{\dagger}_{m\sigma}a_{m\sigma}+\sum_{\mathbf{k}m\sigma}[V(\mathbf{k}m\sigma)a^{\dagger}_{m\sigma}c_{\mathbf{k}\sigma}+\text{H.c.}]+\tfrac{1}{2}U\sum_{\substack{mm'\\ \sigma\sigma'}}{}' n_{m\sigma}n_{m'\sigma'} . \tag{1}$$

Here $\varepsilon_{\mathbf{k}}$ is the dispersion of the (only) band considered, which hybridizes through the third term with the degenerate local f level of energy ε_f (m denoting the orbital quantum number). Electrons on this level are subject to a Coulomb repulsion U. (In the presence of a magnetic field a Zeeman coupling would have to be added which would lift the degeneracy of the band and the localized states in σ and m).

For the following analysis it is useful to simplify, and at the same time to generalize this Hamiltonian in two respects.

(i) In order to account for spin-orbit coupling and crystal-field splitting the quantum numbers m and σ are replaced by μ and ν (see below).

(ii) The band states are grouped into those which, by symmetry, can hybridize with the impurity and those which are decoupled from it. The latter only determine the origin of energy, which does not enter the spectra, whereas the former are labeled by μ, ν, and an energy variable ε. (This transformation is discussed in more detail by Gunnarsson and Schönhammer.[5])

These two steps yield the following Hamiltonian

$$H=\int d\varepsilon\,\varepsilon\sum_{\mu\nu}c^{\dagger}_{\mu\nu}(\varepsilon)c_{\mu\nu}(\varepsilon)+\sum_{\mu\nu}\varepsilon_{f\mu}a^{\dagger}_{\mu\nu}a_{\mu\nu}+\sum_{\mu\nu}\int d\varepsilon[V(\mu\nu,\varepsilon)a^{\dagger}_{\mu\nu}c_{\mu\nu}+\text{H.c.}]+\tfrac{1}{2}\mu\sum_{\substack{\mu\mu'\\ \nu\nu'}}n_{\mu\nu}n_{\mu'\nu'} . \tag{2}$$

Here μ distinguishes the various impurity levels, of degeneracy $N_{f\mu}$, to be taken into account and ν (running from 1 to $N_{f\mu}$) numbers the degenerate states belonging to the energy level $\varepsilon_{f\mu}$ with the degeneracy $N_{f\mu}$. (In the usual theoretical treatments only one such level is considered and its degeneracy is usually denoted by N_f.) The relevant f-electron energies (in zero field) are then denoted as follows: ε_f, the energy of the lowest level considered; $\varepsilon_f+\Delta_{\text{CF}}$, the energy of the higher crystal-field level in the spin-orbit multiplet considered. ($\Delta_{\text{CF}}=0$ if crystal-field effects are neglected.) $\varepsilon_f+\Delta_{\text{s.o.}}$, the energy of the higher spin-orbit level. This level structure incorporates all the available information about the systems considered in this paper.

Two other relevant energies show up in the calculation: The effective hybridization coupling

$$\Delta(\varepsilon)=\pi|\bar{V}(\varepsilon)|^2 \tag{3}$$

involves an average value $\bar{V}$ of $V(\mu\nu,\varepsilon)$. In practice a simple functional dependence of Δ on ε is used (see Sec. II B) which involves an overall coupling strength Δ_0, which will be used in Sec. IV as a measure for the hybridization energy. The lowest energy scale, the "Kondo energy" δ, will be introduced later.

In recent years various theoretical methods have been developed in order to evaluate the physical properties of systems which are governed by the Hamiltonian (1) or (2). Most of them are based on the fact that in the limit of a very large degeneracy ($N_f\to\infty$) of the f level things simplify considerably, and use an expansion in N_f^{-1}. Various reviews have summarized these methods in great detail.[26,27] Here we merely quote the results which are necessary for interpreting various types of spectra and thermodynamic quantities like magnetic susceptibility and specific heat (note that for our purpose the methods discussed in[26,27] had to be generalized in order to account for the multiplet structure mentioned above). The following two quantities have to be calculated: (i) The f spectral function

$$\rho_f(\omega)=-\frac{1}{\pi}\text{Im}\sum_{\mu}\int dt\,e^{i(\omega+i\varepsilon)t}G_f^{(\mu)}(t) \tag{4}$$

with

$$G_f^{(u)}(t)=-i\Theta(t)\langle[a_{\mu\nu}(t),a^{\dagger}_{\mu\nu}(o)]_+\rangle . \tag{5}$$

In the absence of a field and for the usual ν-independent hybridization $G_f^{(\mu)}$ will be independent of the quantum number ν. Thus the sum over μ in Eq. (4) and in the following includes the sum over ν.

(ii) The f-moment spectrum

$$\sigma_f(\omega)=-\frac{1}{\pi}\text{Im}\sum_{\mu}\int dt\,e^{i(\omega+i\varepsilon)t}M_f^{(\mu)}(t) \tag{6}$$

with

$$G_f^{(u)}(f)=-i\Theta(t)\langle[M_{\mu}(t),M_{\mu}(o)]_-\rangle , \tag{7}$$

M_{μ} being the magnetic moment operator associated with the level μ.

These two spectral functions immediately yield the following thermodynamic quantities: the mean occupation of the f level μ,

$$n_f^{(\mu)}(T)=\int d\omega\frac{1}{e^{\beta\omega}+1}\rho_{(f)}^{(\mu)}(\omega) \tag{8}$$

and the magnetic susceptibility

$$\chi(T)=\text{P}\int d\varepsilon\frac{1}{\varepsilon}\sigma_f(\varepsilon) . \tag{9}$$

Moreover $\rho_f(\omega)$ corresponds to the spectrum measured by photoemission ($\omega<E_F$) and bremsstrahlung isochromat spectroscopy (BIS) ($\omega>E_F$), E_F being the Fermi energy.

For arbitrary temperature and for infinite Coulomb repulsion U a "self-consistent diagrammatic large N_f expansion"[26–28] yields, in the so-called "noncrossing" approximation (NCA),[29–33] two coupled integral equations for the quantities $G_0(z)$ and $G_{\mu}(z)$

$$G_0(z)=\left[z-\sum_\mu \int d\varepsilon \frac{\Delta(\varepsilon)}{\pi} G_\mu(z+\varepsilon) f(\varepsilon)\right]^{-1}, \tag{10}$$

$$G_\mu(z)=\left[z-\varepsilon_{f\mu}-\int d\varepsilon \frac{\Delta(\varepsilon)}{\pi} G_0(z-\varepsilon)[1-f(\varepsilon)]\right]^{-1}. \tag{11}$$

Knowing these two auxiliary functions and their imaginary parts, the spectral functions ρ_0 and ρ_μ, one can then evaluate the following quantities: the f partition function

$$Z_f=\int d\varepsilon e^{-\beta\varepsilon}\left[\rho_0(\varepsilon)+\sum_\mu \rho_\mu(\varepsilon)\right]. \tag{12}$$

This yields the thermodynamics of the f electron and, in particular, its contribution to the specific heat; the f-spectral function

$$\rho_f(\omega)=\frac{1}{Z_f}(1+e^{-\beta\omega})\int d\varepsilon \rho_0(\varepsilon) e^{-\beta\varepsilon}\sum_\mu \rho_\mu(\varepsilon+\omega). \tag{13}$$

The photoemission spectrum can be split into a photoemission part ($\rho_f^<$) and a BIS contribution ($\rho_f^>$), see Sec. II B; the f-moment spectral function

$$\sigma_f(\omega)=N_f\sum_\mu \frac{m_\mu^2}{3}\frac{1}{Z_f}\int d\varepsilon\, e^{-\beta\varepsilon}\rho_\mu(\varepsilon) \times[\rho_\mu(\varepsilon+\omega)-\rho_\mu(\varepsilon-\mu)], \tag{14}$$

where m_μ is the magnetic moment of level μ.

At $T=0$ the variational approach by Gunnarsson and Schönhammer[5] yields a more direct insight into the structure of the ground state and of the spectral functions $\rho_f^<$ and $\rho_f^>$. This method also has the advantage of being extensible to the finite-U case (generalization of NCA to $U<\infty$ have also been put forward more recently).[34] Although the limit $T\to 0$ of the NCA equations is somewhat tricky (see Sec. II B for a few remarks and references), the spectra calculated by NCA for very low temperatures and those obtained for the same system at $T=0$ using the variational approach are essentially identical. Within the variational approach the Kondo energy δ, mentioned before, and thus the Kondo temperature $T_K=\delta/k_B$, can be directly identified in the calculation of the ground-state energy E_G: for the lowest-order (in N_f^{-1}) wave function δ is the "binding energy" of the impurity, i.e., E_G is given by

$$E_G=E_{\rm FS}+\varepsilon_f-\delta, \tag{15}$$

$E_{\rm FS}$ being the energy of the filled Fermi sea of band states. (In NCA the Kondo energy has to be identified from the numerically evaluated form of the f-spectral function, see the end of Sec. II B). The quantity δ is given by the (largest) solution of

$$\delta=\varepsilon_f-\int \frac{d\varepsilon}{\pi}\frac{N_f\Delta(\varepsilon)}{\varepsilon-\delta}. \tag{16}$$

In the Kondo limit, where the bare f level lies well below the Fermi energy (and the hybridization is not too strong) the solution of (16) is given by the well-known expression (which is nonanalytic in δ_0 at $\Delta_0=0$):

$$\delta=\frac{N_f\Delta_0}{\pi}e^{\pi\varepsilon_f^*/N_f\Delta_0} \tag{17}$$

with the renormalized f energy

$$\varepsilon_f^*=\varepsilon_f+\frac{N_f\Delta_0}{\pi}\ln\frac{\pi|B|}{N_f\Delta_0}. \tag{18}$$

This result is valid for a constant band density of states (of rectangular shape), B being the energy of the lower band edge (counted from the Fermi energy, which is the reference energy, i.e., the "zero," of all our calculations).

The Kondo energy also shows up in the zero-temperature susceptibility,[5] which is, to lowest order in N_f^{-1}:

$$\chi(T=0)=\frac{1}{3}\frac{(N_f+1)(N_f-1)}{4}m_\mu^2\frac{n_f(T=0)}{k_BT_k} \equiv\frac{1}{3}\frac{\bar\mu^2 n_f(T=0)}{k_BT_k}. \tag{19}$$

[We have replaced the usual angular momentum quantum number J by $(N_f-1)/2$, such that $J(J+1)$ becomes $\frac{1}{4}(N_f-1)(N_f+1)$.] For the two cases considered the magnetic momentum m_μ has the following values.

(i) Spin-orbit ground state with $J=\frac{5}{2}$ or $\frac{7}{2}$ (i.e., $N_f=6,8$): $m_\mu=q_J\mu_B$; g_J being the corresponding g factor.

(ii) The crystal-field Γ_7 ground state (i.e., $N_f=2$): $m_\mu=\frac{5}{3}g_J\mu_B$. Thus $\bar\mu=\frac{5}{6}\sqrt{3}g_J\mu_B$, as one easily verifies using the well-known linear combination of spin-orbit eigenstates that form a basis in the Γ_7 subspace.

B. Model calculations

The coupling of the localized level with the conduction electrons has been modeled by a smooth function of energy rather than taking into account the full structure, which only could come from an *ab initio* band-structure calculation. For some compounds a semielliptic band shape

$$\Delta(\varepsilon)=\frac{\Delta_0}{\pi}\left[1-\left[\frac{\varepsilon-\varepsilon_c}{b}\right]^2\right]^{1/2} \tag{20}$$

was found to be appropriate. b sets the width of the band, ε_c the center of the band, and Δ_0 the nominal hybridization strength. This type of band shape tends to give a strong ionization peak. For other compounds a Lorentzian band shape

$$\Delta(\varepsilon)=\frac{\Delta_0}{\pi}\left[1+\left[\frac{\varepsilon-\varepsilon_c}{b}\right]^2\right]^{-1} \tag{21}$$

was chosen. This band shape tends to minimize the strength of the ionization peak. Finally, a Gaussian shape

$$\Delta(\varepsilon)=\frac{\Delta_0}{\pi}e^{-[(\varepsilon-\varepsilon_c)/b]^2} \tag{22}$$

offers a compromise concerning ionization peak strength and facilitates windowing in calculating the Green's functions.

The Green's functions G_0 and G_μ determine, in principle, the dynamical properties we are interested in. However, direct calculation of Boltzmann weighted spectral functions $b(\omega)=e^{-\beta(\omega-\varepsilon_0)}(1/\pi)\mathrm{Im}[G_0(\omega)]$ and $a_\mu(\omega)=e^{-\beta(\omega-\varepsilon_0)}(1/\pi)\mathrm{Im}[G_\mu(\omega)]$ seems essential to obtain numerically significant results since the imaginary parts of the spectral functions vanish exponentially fast below threshold. The energy ε_0 is introduced for computational convenience. The results do not depend on ε_0, in principle, however, the accuracy of the f-partition function is quickly lost when ε_0 is outside a small range at the threshold energy. The self-consistent equation[35]

$$b(\omega)=|G_0(\omega-i0)|^2\sum_\mu\int\frac{\Delta(\varepsilon)}{\pi}a_\mu(\omega+\varepsilon)[1-f(\varepsilon)]d\varepsilon \tag{23}$$

$$a_\mu(\omega)=|G_\mu(\omega-i0)|^2\int\frac{\Delta(\varepsilon)}{\pi}b_\mu(\omega-\varepsilon)f(\varepsilon)d\varepsilon \tag{24}$$

yield accurate Boltzmann-weighted functions up to a normalization constant. We have chosen to renormalize a and b with the f-partition function such that

$$1=\int\left[b(\varepsilon)+\sum_\mu a_\mu(\varepsilon)\right]d\varepsilon\ . \tag{25}$$

The f-partition function Z_f can be calculated by

$$Z_f=\frac{1}{\pi}\mathrm{Im}[G_0(\varepsilon_0-i0)]/b(\varepsilon_0)$$
$$=\frac{1}{\pi}\mathrm{Im}[G_\mu(\varepsilon_0-i0)]/a_\mu(\varepsilon_0)\ , \tag{26}$$

where ε_0 is chosen to maximize numerical accuracy. The two sets of self-consistent equations have been solved on the real axis using fast-Fourier transform to execute the convolutions. The temperature, which remains always finite in these calculations, serves for smoothing and band limitation of the spectral functions. The size of the energy window was enlarged to the point where window-size effects were no more noticeable. At this window size the imaginary parts of the spectral functions reach a minimum value which is drowned in the roundoff error.

The spectral density relevant for ultraviolet photoelectron spectroscopy (UPS) can be written

$$\rho^<(\omega)=\frac{1}{\pi}\sum_\mu\int a_\mu(\omega+\varepsilon)\mathrm{Im}[G_0(\varepsilon-i0)]d\varepsilon\ . \tag{27}$$

The spectral density appropriate for BIS is

$$\rho^>(\omega)=\frac{1}{\pi}\sum_\mu\int\mathrm{Im}[G_\mu(\omega+\varepsilon-i0)]b(\varepsilon)d\varepsilon \tag{28}$$

using the normalized a and b functions. We identify the position of the first peak at positive energy of the function $\rho(\omega)=\rho^<(\omega)+\rho^>(\omega)$ with the Kondo temperature T_0 of the system.

Some of the spectral functions were calculated using the Gunnarsson Schönhammer (GS) approach.[5] Both NCA and GS methods yield approximate spectral functions for Hamiltonian (1), NCA for finite temperature, and GS for zero temperature. For heavy-fermion compounds the instrumental broadening (including also an artificial temperature broadening in the GS case) masks features on the Kondo and crystal-field energy scale. To the experimentally accessible resolution both methods agree except for a difference in the actual value of T_K taken as the peak position of the f-spectral density in the NCA and according to Eq. (16) in the GS method. Also in the case of strong hybridization the two methods agree, as experiment remains in the low-temperature limit. In the intermediate case as exemplified by $CeSi_2$ the NCA is the appropriate approach to study the disappearance of the low-temperature spectral peaks.

III. THE SINGLE-IMPURITY MODEL APPLIED TO PHOTOEMISSION OF 4f STATES

A. Qualitative discussion of the excitation spectra

In the atomiclike limit the 4f states can be simply considered as weakly bound core levels showing in addition all the manifestations of the multiplets which can occur in a partly filled shell.[12] The 4f-population changes induced by a photoemission process or an inverse-photoemission process correspond to discrete increases of the total energy E_t. These excitation energies can be accurately calculated within the renormalized-atom scheme as many-electron energy differences between initial and final states.[36] The excitation spectrum $S(E_t)$ of a metallic sample containing localized f states without multiplet splitting is shown in Fig. 1(a).[11] The total energy of the ground-state configuration f^n is identified with the Fermi level (E_F) taken as reference of the energies. In order to

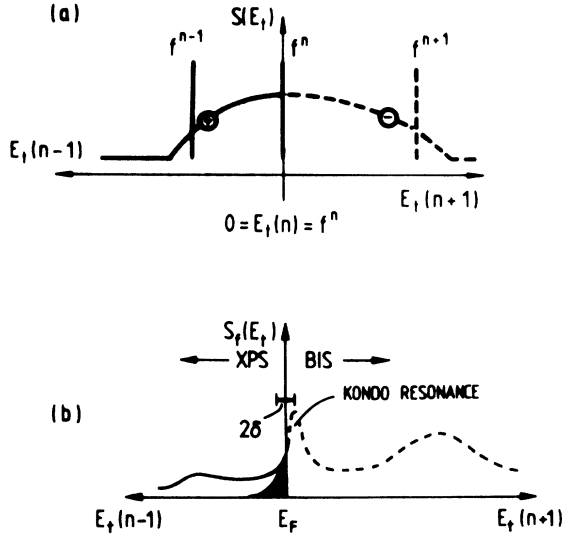

FIG. 1. (a) Excitation spectrum $S(E_t)$ of unhybridized 4f and band states as a function of the total final-state energy E_t. The ground state f^n chosen as an origin of E_t does not belong to $S(E_t)$. (b) Excitation spectrum of 4f states hybridized with a metallic band in the case of a Ce impurity (after Ref. 7). Solid line (XPS), excitations after emission of one electron. Dashed line (BIS), excitations after addition of one electron. Dark peak, low-energy excitations within the energy range δ.

be compatible with the traditional single-electron representation, the total transition energies for emission or addition of one electron are represented in opposite directions, although they are both positive. The sum of the energies of the two states f^{n-1} and f^{n+1} can be visualized as corresponding to the following transition between two independent atoms within the solid, $4f^n+4f^n \rightarrow 4f^{n+1} \rightarrow f^{n-1}$ which defines Coulomb correlation energy U_{ff}.[12] On the other hand, the band states show an excitation spectrum which is continuous across E_F (solid line for electron emission and dashed line for electron addition). This means that at the Fermi energy the population of Bloch states can be modified for an infinitely small excitation energy.[37] The relative energy position between $4f$ and band excitations is fixed but in this limit no mixing takes place between these states which keep their distinct characters.

In the case of Ce [$n=1$ in Fig. 1(a)], the energy position between f^0 and f^1 is ε_f. When the hybridization between f states and band states is taken into account the total energy is lowered by a small energy δ defining the Kondo temperature $T_K=\delta/k_B$. This mixing involves a decrease of the f count ($n_f<1$) and the formation of band holes which must be concentrated within an energy range of about δ above E_F in order to allow an energetically favorable hybridization. In the many-body ground state, the strong weight of f-symmetry states admixed to band states within δ is the occupied part of the Kondo peak. The parameter δ defines the relevant energy scale for all low-energy phenomena associated with the weakly hybridized $4f$ states. This peculiar ground state is reflected by the characteristic excitation spectrum represented qualitatively in Fig. 1(b). The spectral function $S_f(E_t)$ accounting only for the $4f$ signal is always superimposed on a bandlike spectrum assumed to have a simple analytical shape, for example, in Fig. 1(a). The analysis of the spectral function for photoemission shows that within δ above E_F, the final-state distribution (black peak) is proportional to the weight to the f-projected states forming the many-body ground state. The essential difference is that the integrated intensity of this peak in the photoemission spectrum is $n_f(1-n_f)$ whereas the f weight in the ground state is n_f. In Ce systems where the hybridization is usually weak, n_f is very close to one. This means that in the photoemission spectra, only a narrow and weak peak at E_F reflects directly the peculiarity of the electronic structure responsible for the heavy-electron manifestations. This tiny replica of the Kondo resonance corresponds to photoemission final states having practically the initial f population. At higher energies above E_F the final states have a character quite different from the ground state. The broad peak is reminiscent of the f^0 final state in the atomiclike limit (ionization peak) and it has an antibonding character.

In the excitation spectrum where one electron is added (inverse photoemission), a rather similar situation is observed but now the integrated intensity is $14-n_f$ and the top of the Kondo resonance is located at δ above E_F. The situation depicted by the dashed curve in Fig. 1(b) corresponds qualitatively to the case of Ce. In heavy rare-earth systems where hybridization effects can be also important, one can take advantage of the mirror properties of an atomic shell with respect to its half population and the spectra accounting for the emission or the addition of one electron can be exchanged.[6]

When the spin-orbit interaction of the f electrons is included, the situation already becomes more complicated, even in the simplest case of Ce. Without hybridization and at $T=0$, the ground state corresponds now to the $f^1_{5/2}$ level with a degeneracy N_f which is decreased from 14 to 6. When one electron is removed, the relevant f excited states which need to be considered within the atomiclike limit are the $f^1_{5/2}$ and $f^1_{7/2}$ states with one band hole at E_F and the f^0 state with the band filled up to E_F. As previously the superimposed band excitations appear as a continuum reflecting the single-particle density of states modulated by the matrix elements. Curve (*b*) of Fig. 2 shows this excitation spectrum as a function of the total energy $E_t(N-1)$ referenced to the ground-state energy as in Fig. 1(a). If the hybridization is switched on, the ground state will acquire only a negligible contribution of $f^1_{7/2}$ character since in all Ce systems δ is much smaller than the spin-orbit splitting $\Delta_{s.o.}=280$ meV. The

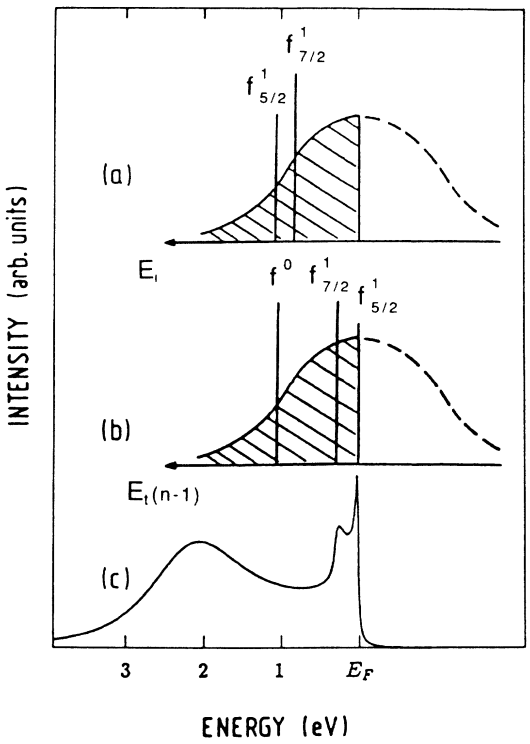

FIG. 2. Curve (*a*), schematic representation of the single-particle excitation energies (E_t) of $4f$ and band states without hybridization. The vertical bars indicate the energy gained by an electron initially at E_F when it is placed into the $4f^1_{5/2}(\varepsilon_f)$ or into the $4f^1_{7/2}(\varepsilon_f-\Delta_{s.o.})$ level. (*b*), total-energy representation of the band states and of the relevant f-excited states in the atomic limit [cf. Fig. 1(a)]. The vertical bars indicate the $4f^1_{5/2}$ and $4f^1_{7/2}$ states with one band hole at E_F and the $4f^0$ state with the band filled up to E_F. (*c*), calculated (GS, $T=0$) excitation spectrum of the $4f^1$ states, including the spin-orbit splitting $\Delta_{s.o}=280$ meV and the hybridization with a metallic band after emission of one electron [cf. Fig. 1(b), XPS].

corresponding spectral function for photoemission shown in curve (*c*) of Fig. 2 is very similar to the one of curve (*b*), it contains only an additional peak accounting for final states of $f^1_{7/2}$ character. One can go one step further and include the splitting of the $f^1_{5/2}$ and $f^1_{7/2}$ states in the crystal field (CF). One should add these discrete levels in curve (*b*) and now, depending on the relative orders of magnitude of Δ_{CF}, δ, and $k_B T$, the initial state can consist of the lowest CF level or of a mixture of CF levels. Photoemission spectra can be expected to reflect such excitations but these have usually an energy separation smaller than the instrumental resolution and can be broadened by short lifetimes. The influence of the crystal-field splitting on the measured spectra is a rather critical problem which will be discussed later (Sec. II B) on the basis of a model calculation in which it is included.

One can also describe the excitation of a system without hybridization as a function of the binding energies E_i of single particles, as shown in curve (*a*), Fig. 2. The zero energy of the electrons is taken at the Fermi energy. Then, starting from an f^0 configuration, the vertical bars indicate the energy gained by an electron initially at E_F when it is placed into the $f^1_{5/2}$ level (ε_f) or into the $f^1_{7/2}$ level ($\varepsilon_f - \Delta_{s.o.}$). The same definition applies for the occupation of band states forming the continuum. This representation has the advantage to be very closely related to the structure of the single-impurity Hamiltonian. On the other hand, the total-energy representation [curve (*b*), Fig. 2] shows more directly the states involved in the hybridization and the nature of the excited states observed in the spectroscopies.

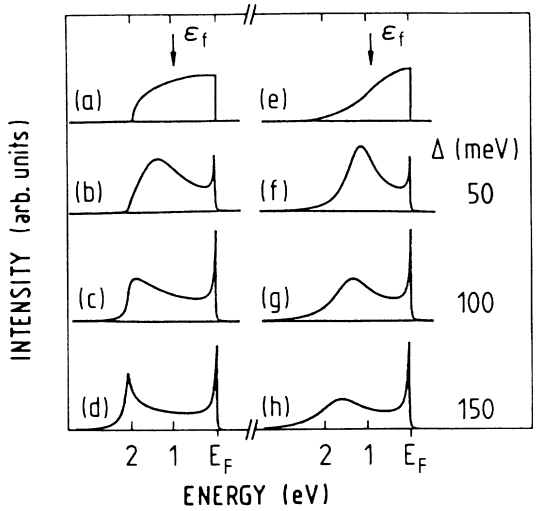

FIG. 3. Influence of the conduction-band shape [(*a*), semielliptical; (*e*) Lorentzian] on the excitation spectra: (*b*)–(*d*) and (*f*)–(*h*), *f*-spectral functions for the two cases calculated within the GS formalism (without spin-orbit coupling) for increasing values of the hybridization strength Δ and the constant value of ε_f indicated by the arrow.

B. Influence of the parameters on the excitation spectra

1. Shape of the conduction band

If constant hopping matrix elements between the *f* orbital and the conduction states are assumed, the energy dependence of the coupling strength is simply given by the density of the band states. In the ground state, the hybridization is important only within the energy range δ above E_F which is very small compared with the bandwidth. For this reason it is sufficient to use the constant coupling strength at E_F to describe the Kondo resonance. On the contrary, the spectral function at higher energies can depend rather critically on the particular band shape assumed in the model. These facts are illustrated in Fig. 3 where spectral functions calculated with a semielliptical [curve (*a*)] and a Lorentzian [curve (*e*)] band shape (see Sec. II B) are compared for increasing values of Δ and the constant value of ε_f indicated by the arrow. The spin-orbit coupling has not been included in these model calculations. As expected, for the same value of Δ but different band shapes, the peak of low-energy excitations near E_F remains unchanged. For the semielliptical band shape, the maximum of the broad hump moves surprisingly fast towards higher energies when Δ increases. For the largest hybridization strength $\Delta = 150$ meV [curve (*d*), Fig. 3], a sharp accumulation of excitations around the bottom of the band is observed. This behavior originates from the vertical onset of the semielliptical band and not from a numerical problem. In photoemission spectra we do not observe such pronounced structures and generally a Lorentzian band shape is found to provide a more realistic simulation of the data. It should be noted that with increasing hybridization, the antibonding f^0-like excitations are moving away from the ionization peak corresponding to $\Delta = 0$, so that a simplistic determination of ε_f from the high-energy peak position will always yield an overestimated value of this parameter. Furthermore, one must be aware that a realistic calculation of the spectral function in the high-energy range can only be performed if the real density of band states available for hybridization is known.

2. Spin-orbit and crystal-field splitting

As mentioned previously, the $4f^1$ level without any splitting mechanism would have a degeneracy $N_f = 14$. With spin-orbit splitting the lowest state ($f^1_{5/2}$) has a degeneracy $N_f = 6$ which can be further reduced to $N_f = 4$ or 2 in the crystal field, depending on the local symmetry. When all other parameters are fixed, this dramatic variation of N_f leads to very different values of n_f and δ. Obviously when model calculations including both types of interaction are fitted to the spectra, more realistic values of the low-energy scale δ characterizing the ground state are obtained. Figure 4 shows the evolution of the *f* spectral function for the fixed parameters $\varepsilon_f = -1$ eV and $\Delta = 100$ meV, when successively the spin-orbit interaction ($\Delta_{s.o.} = 300$ meV) and the crystal-field interaction ($\Delta_{CF} = 35$ meV between the two lowest states) are activated in the model calculation. The striking feature in this figure is the enormous weight transfer from the Kondo resonance obtained for the fully degenerate case with

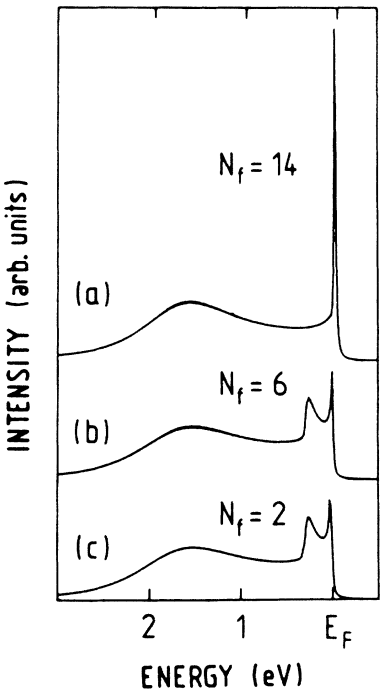

FIG. 4. Evolution of the f-spectral function, calculated within the GS model for the fixed parameters $\varepsilon_f = -1$ eV and $\Delta = 100$ meV for different degeneracies N_f of the ground state: (a) without spin-orbit splitting, (b) with spin-orbit interaction $\Delta_{s.o.} = 300$ meV, (c) with $\Delta_{s.o.} = 300$ meV and crystal-field interaction $\Delta_{CF} = 35$ meV between the two lowest states. An instrumental resolution of 20 meV FWHM is included in the calculation. Note that curves (b) and (c) are nearly indistinguishable.

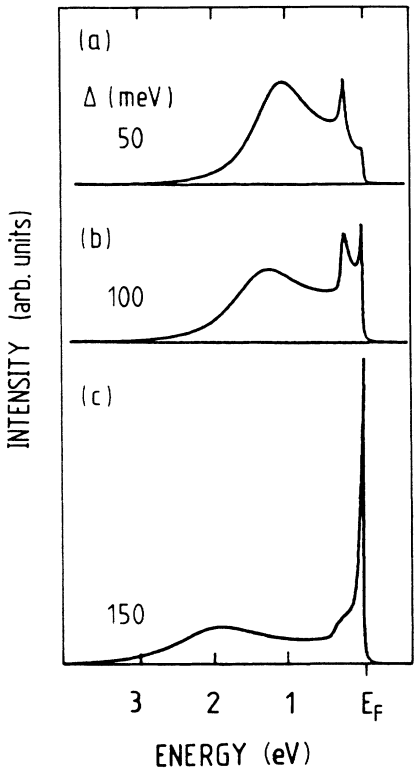

FIG. 5. (a)–(c) influence of the hybridization strength Δ on the f spectra calculated with the parameters $\varepsilon_f = -1$ eV, $\Delta_{s.o.} = 300$ meV, $\Delta_{CF} = 30$ meV (between the two lowest levels) within the GS model. The instrumental broadening of 20 meV is taken into account.

$N_f = 14$ [curve (a), Fig. 4)] to the higher component $f^1_{7/2}$ when the spin-orbit interaction is included into the calculation [curves (b) and (c) of Fig. 4]. The consequence of the crystal-field splitting can practically not be discerned at the energy scale of curve (c) but in fact a very important intensity transfer occurs also to the first excited crystal-field level above the ground state. (This effect will be illustrated later in the discussion of $CeSi_2$). This similarity of curves (b) and (c) of Fig. 4 demonstrates that when the resolution is not quite sufficient to resolve this splitting, the "true" Kondo resonance cannot be discerned as an isolated peak at E_F. This means that without crystal-field splitting good fits to the spectra can be obtained, but incorrect values of δ and n_f are deduced.

3. Hybridization

In Fig. 5 we illustrate the influence of the hybridization strength Δ on the f spectra calculated with the following constant values of the parameters: $\varepsilon_f = -1$ eV, $\Delta_{s.o.} = 300$ meV, and $\Delta_{CF} = 30$ meV (between the two lowest levels). For the largest hybridization strength $\Delta = 150$ meV [curve (c) of Fig. 5], a strong intensity is concentrated on the narrow Kondo peak which has the weight $n_f(1-n_f)$ while the excitations to the $f^1_{7/2}$ levels and the states with f^0 character are not very pronounced in this spectrum. This situation is not too far from a conventional metallic state where only a f band pinned at E_F should be observed. When the value of Δ becomes smaller, the relative intensity of the Kondo peak decreases for the benefit of the more atomiclike excitations at higher energies. The intensity distribution among these final states can hardly be predicted intuitively but needs to be calculated with the model [curves (a) and (b) of Fig. 5]. For a very weak hybridization the excited spin-orbit component and crystal-field levels [not resolved in Fig. 5(a)] survive at the expense of the Kondo peak which is no longer observable. In the purely localized limit ($\Delta = 0$), the low-energy excitations would disappear completely, leaving only an atomiclike f^0 peak at ε_f.

4. Temperature

In the different situations discussed previously we have implicitly assumed $T = 0$ K. In experiments this condition can be approximatively satisfied for $T < \delta/k_B$, a temperature range that we can only reach at the present time for moderately heavy electrons. In order to make a valuable comparison between theory and experiments, it is important to investigate the influence of finite temperatures on the spectra. Curves (a)–(d) of Fig. 6 shows for a typical Kondo regime ($\varepsilon_f = -1$ eV, $\delta = 3$ meV) the temperature dependence of the f spectral function calculated with the NCA. It takes into account a spin-orbit splitting of 300 meV, a crystal-field splitting of 35 meV be-

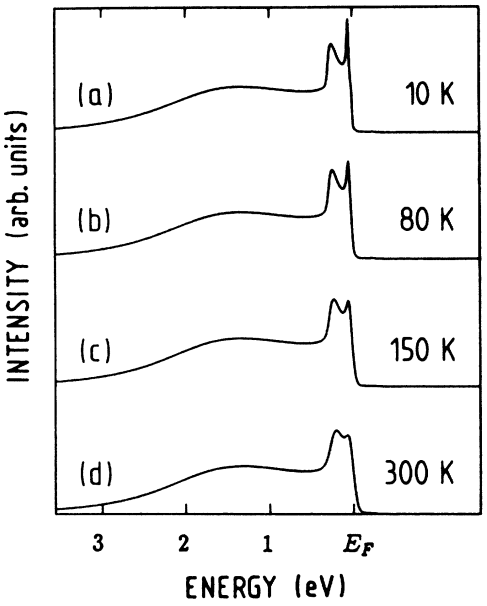

FIG. 6. Curves (*a*)–(*d*), temperature dependence of the *f*-spectral function for a typical Kondo regime ($\varepsilon_f = -1$ eV, $\delta = 3$ meV) calculated within the NCA taking into account a spin-orbit splitting of $\Delta_{s.o.} = 300$ meV, a crystal-field splitting of $\Delta_{CF} = 35$ meV between the two lowest states, and an instrumental broadening of 20 meV.

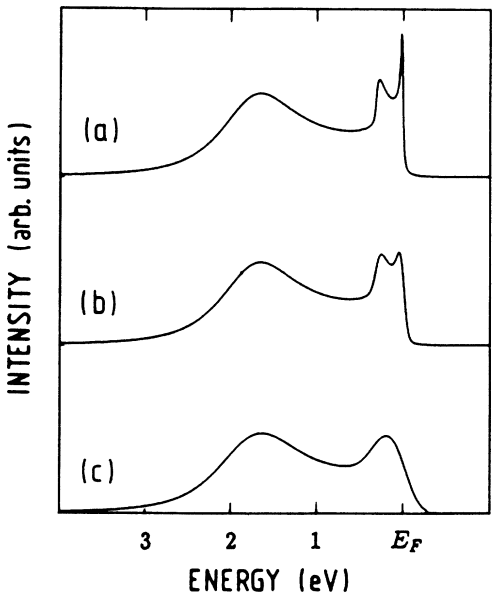

FIG. 7. Influence of the instrumental resolution on the shape of the excitation spectra. A typical GS spectral function ($\varepsilon_f = 1.2$ eV, $\Delta = 100$ meV, $\Delta_{s.o.} = 300$ meV) has been convoluted with Gaussian resolution functions of different FWHM: (*a*) 20 meV, (*b*) 100 meV; and (*c*) 400 meV.

tween the lowest states, and an instrumental broadening of 20 meV. Since the Kondo temperature is 35 K, the spectral function at 10 K shown in curve (*a*) does not contain any temperature contribution discernable at this scale. In this case the Kondo peak reflects essentially the formation of a singlet ground state. When the temperature increases above T_K, we observe a flattening of the Kondo peak corresponding to the gradual population of nonsinglet states. It is also interesting to notice that the structure originating from the $f^1_{7/2}$ state is also attenuated at high temperature. In fact the *f* population n_f does not vary markedly in the temperature range considered in Fig. 6 and the calculation shows that the relative weight of low- and high-energy *f* excitations is not modified in the different spectra.

5. *Instrumental resolution*

Finally in Fig. 7 we illustrate the influence of the instrumental resolution on the shape of the spectra. In order to simulate the conditions encountered in high-resolution UPS, conventional UPS, and x-ray photoelectron spectroscopy (XPS), we have convoluted a typical spectral function ($\varepsilon_f = -1.2$ eV, $\Delta = 100$ meV, $\Delta_{s.o.} = 300$ meV) with a Gaussian line of (a) 20 meV, (b) 100 meV, and (c) 400 meV at full width at half maximum (FWHM), respectively. It is not surprising that the Kondo peak and the $4f^1_{7/2}$ excitations, which are clearly separated at high resolution [curve (*a*), Fig. 7], form a featureless hump which could be interpreted as accounting for a single peak centered at a suitable energy above E_F when the resolution becomes worse than the spin-orbit splitting [curve (*c*)]. This simple example emphasizes the necessity of a high-energy resolution in order to extract from the spectra reliable information on the low-energy excitations reflecting within δ the nature of the ground state.

IV. EXPERIMENTAL DETAILS

The photoemission measurements were performed in an apparatus combining UPS, XPS, BIS or inverse photoemission, and electron energy-loss spectroscopy.[16] The spectra presented in this paper have been exclusively obtained with high-resolution UPS but other techniques have been used in some cases to characterize the samples. The instrumental resolution of UPS is mainly determined by the linewidth of the photon source and the resolving power of the electron analyzer. The spectra are excited by the main resonance lines at 21.2 eV (He I) and 40.8 (He II) produced in the gaz discharge of a commercial lamp. The light is guided in a 200-mm-long and 1-mm-diameter quartz capillary with three differential pumping stages. The He pressure in the gaz discharge is of the order of 0.1 Torr, it falls to 10^{-3} Torr in the first pumping stage and a pressure of 10^{-10} Torr can be maintained in the analysis chamber. The resonance lines have an intrinsic width of the order of 1 meV which sets the ultimate value of the obtainable resolution.[38] For the He I line the self-absorption can induce a line broadening which can reach several meV. This disturbing effect can be minimized by using a short discharge column and maintaining the pressure in the discharge as low as possible.[38]

For our electrostatic hemispherical analyzer with a mean radius $R = 5$ in., the resolution ΔE can be estimat-

ed from the expression $\Delta E = ES/2R + f(\theta)$, where E is the pass energy, S is the sum of the entrance and exit slit dimensions in the dispersion direction, and $f(\theta)$ is a function of the acceptance angle of the analyzer. Theoretically by using a preretardation of the electrons before the lense which has a fixed retarding ratio of 20, one could reach at the expense of the intensity an arbitrarily small resolution. In practice, however, the resolution is limited by the lowest pass energy for which the different perturbations in the spectrometer induce deviations of the electron trajectories comparable to the slit widths. In order to optimize the resolution of our instrument we have taken the following precautions. (i) even weak magnetic materials in the sample region and in the spectrometer have been eliminated or demagnetized, (ii) external magnetic fields have been screened by μ-metal shields, (iii) all voltages applied to the lenses and to the analyzer have been carefully stabilized and their ripple filtered to better than 1 meV. In this way we obtain a stable and reproducible resolution slightly better than 20 meV in the spectra of solid samples. This performance is demonstrated in Fig. 8 by the spectrum of Ag excited with He II. For a pass energy of 3 eV and a sample temperature of 15 K, we observe a total width of the Fermi edge of 19 meV.

The elements Ce and Yb were evaporated *in situ* from a resistively heated tungsten coil on a sapphire substrate in contact with the cold finger of a closed-cycle He refrigerator. The oxide contamination was monitored via the intensity of the O $2p$ emission at about 6 eV binding energy, using the He II line of $h\nu = 40.8$ eV. Repeated evaporations are necessary to obtain oxygen-free sample surfaces. The compounds $CeCu_6$, $CeAl_2$, and $CeSi_2$ were prepared by melting together stoichiometric amounts of the constituents in a levitation furnace. The $YbAl_3$ sample was grown from Al flux in a evacuated Al_2O_3 crucible.[23] The crystallographic structure of the polycristalline samples was confirmed by x-ray-diffraction analysis. The sample surfaces were cleaned by repeated scraping with an Al_2O_3 file in the electron spectrometer. The CeN sample was prepared *in situ* by evaporation of Ce on a tungsten substrate held at 500 °C in a nitrogen atmosphere of 10^{-6} Torr. Subsequently the sample was annealed for a few seconds at 1200 °C. This procedure was essential in order to obtain a homogeneous film, as verified by comparison of the photoemission spectra with those obtained from a CeN single crystal of an earlier study.[39]

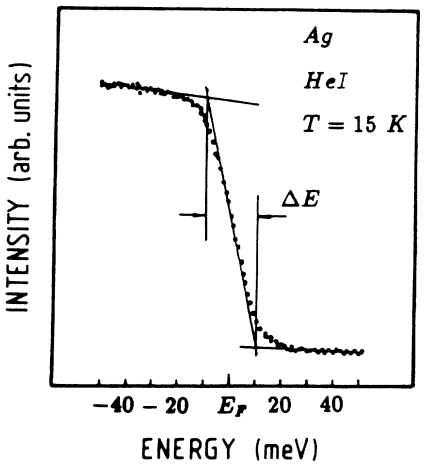

FIG. 8. Illustration of the experimental resolution: photoemission spectra of the Fermi edge of Ag at 15 K. The step between the data points is 1 meV and the total width of the Fermi edge is 19 meV.

V. CASE STUDIES

A. The γ-α phase transition of Ce metal

The puzzling problem of the γ-α isostructural phase transition of Ce metal has been studied with electron spectroscopies during more than one decade and the results have been interpreted by controversial models.[40] Figure 9 shows two different sets of photoemission spectra of α- and γ-Ce compared with the $4f$ intensity obtained from a single-impurity model calculation. Curves A have been measured with a resolution of 0.12 eV.[41] They display the two well-known $4f$ peaks, one at about E_F and the other one at energies somewhat larger than 2 eV. The less bound peak has a rather different form and position in the two phases: in α-Ce it is rounded but seems to be cut by the Fermi energy while in γ-Ce it is much sharper and has its maximum at 0.2 eV. This variation seems to be in contradiction with the single-impurity model predicting that the occupied part of the Kondo peak is always maximum at E_F. The origin of this misleading observation is revealed by the spectra B measured with a resolution of 20 meV.[16] The single

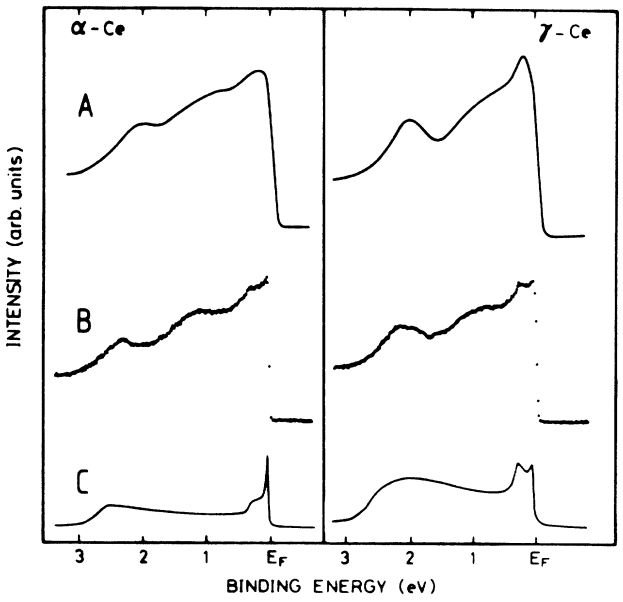

FIG. 9. Photoemission spectra of α- and γ-Ce. A, measured at the photon energy $h\nu = 40.0$ eV with a resolution of 120 meV (Ref. 41); B, measured at the photon energy $h\nu = 40.8$ eV with a resolution of 20 meV (Ref. 16). Curve C, model calculation of the $4f$-intensity within the GS formalism (Ref. 16).

peaks observed near E_F at low resolution show now two structures, one at E_F, the other one at 280 meV. Their intensity ratios are quite different in α- and γ-Ce. These new features result from the spin-orbit splitting giving rise to the two terms $f^1_{5/2}$ and $f^1_{7/2}$ separated by 280 meV. In the model calculation of the $4f$ intensity (curves C) these two multiplets have been taken into account. A very good reproduction of the measured $4f$ intensity near E_F is obtained. The γ-α transition is then simply simulated in the model by a 30% increase of the hybridization strength corresponding to a change of δ from 5 to 25 meV (or of n_f from 0.97 to 0.88). Figure 10 shows with more detail this range of low-energy excitations. Curves A represent now the experimental $4f$ intensity obtained by subtraction of weighted spectra measured with 40.8 and 21.2 eV photon energy.[16] The agreement with the calculated spectral functions B is gratifying. The shaded peaks correspond to the occupied part of the Kondo peak [black peak in Fig. 1(b)] broadened by the thermal and instrumental contributions. One has to notice that the relative intensities in the spectra of α- and γ-Ce have been arbitrarily normalized to about the same intensity of the Kondo peaks. The structure originating from the $f^1_{7/2}$ level is in fact decreasing more slowly than the Kondo peak in the $\alpha \rightarrow \gamma$ transition and in very weakly hybridized systems it can remain observable while the Kondo peak is no longer detectable (see Sec. III C, Fig. 6).

In the complete spectra shown in Fig. 9 the agreement between the measurements and the model calculations is only qualitative for the location and shape of the high-energy $4f$ peak. As discussed in Sec. III A, this must be attributed to the fact that the real density of band states has been simulated by a simple and smooth function in the model calculation. Nevertheless, we believe that the high-resolution spectra[16] analyzed within the single-impurity model demonstrate that the hybridization increase is the essential mechanism driving the $\gamma \rightarrow \alpha$ transition.[42] Another confirmation of the validity of this approach has been provided by the variation of the core levels and BIS spectra concomitant to the $\gamma - \alpha$ phase transition of Ce metal.[43]

B. CeN—a narrow-band material

The compound CeN shows unusual properties[44,45] and it was concluded from previous spectroscopic measurements[39,46] that these were likely to be attributed to a fluctuation between the two nearly degenerate configurations f^0 and f^1. In fact, a careful single-impurity analysis of different spectroscopic results shows that the energy separation ε_f between these two uncoupled configurations is of the order of 1 eV whereas the hybridization strength is about 10 times smaller than ε_f. These values seem to be incompatible with a fluctuation mechanism so that a new high-resolution photoemission study of CeN has been performed with He I and He II radiation at 30 K.[18] Figure 11 shows an UPS spectrum in the range between the top of the full p band and E_F. It is compared to a model calculation including the spin-orbit interaction which yields an f population $n_f = 0.82$ and an energy lowering $\delta = 15$ meV. The featureless lowest line represents the conduction band assumed in the calculation; its relative intensity in the spectrum has been determined from the atomic cross-section ratios for f and p states at the He II photon energy.[18] The striking similarity between measured and calculated spectra yields an indisputable demonstration that the model used contains the essential ingredients for describing these electronic excitations in CeN.

C. Temperature dependence of the Kondo resonance in $CeSi_2$

In order to investigate the temperature dependence of the Kondo peak one has to look for systems where its intensity $n_f(1-n_f)$ is not too weak and T_K lies within the temperature range accessible to the experiment. The compound $CeSi_2$ appears to be suitable for this kind of study since the linear coefficient of its specific heat is

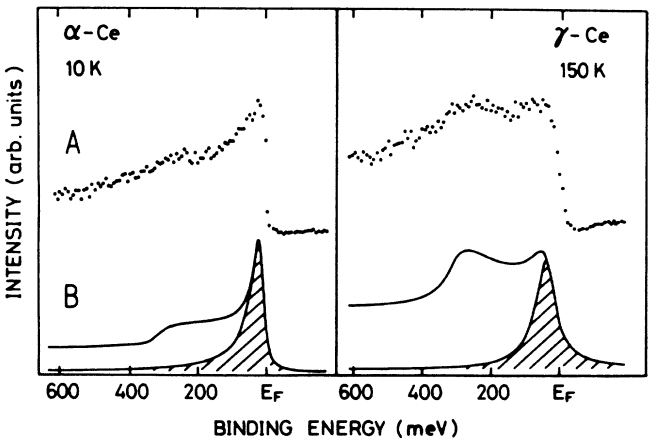

FIG. 10. Low-energy $4f$ excitations in the photoemission spectra of α- and γ-Ce (Ref. 16). A, experimental contribution obtained from the difference of the spectra excited with the He II and He I lines. B, model calculation of the $4f$ intensity (GS) (Ref. 16).

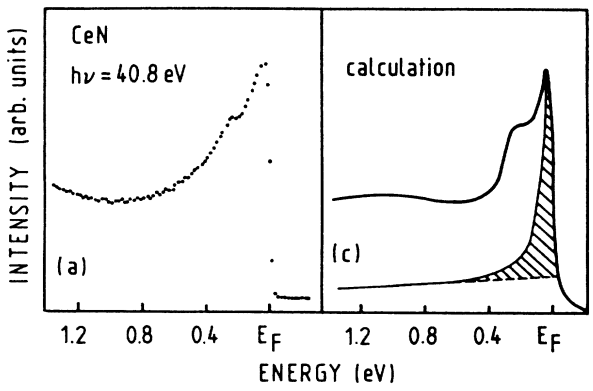

FIG. 11. Low-energy $4f$-excitations in the photoemission spectra of CeN. (a), experiment; (b), model calculation (GS). The dashed line indicates the contribution from other symmetries (Ref. 18).

enhanced by a factor of 100 as compared to the free-electron model, i.e., it is 1 order of magnitude smaller than in the most extreme heavy-electron systems. Furthermore, no magnetic order has been observed in this compound.[47–49] Figure 12(c) shows the uv photoemission spectrum of $CeSi_2$ measured at 15 K with a resolution of 40 meV.[22] The nature of the different peaks is the same as in the previous examples and the dashed line indicates the estimated contribution of the band states. Curve *D* shows that a good simulation of the experimental $4f$ contribution is obtained for $\delta = 3$ meV ($T_K = 35$ K) and $n_f = 0.97$. The spectrum *B* of Fig. 12 represents the $4f$ contribution deduced from the difference of two spectra measured with synchrotron radiation at the maximum and minimum of the Fano resonance curve.[15] It shows at the right position the broad peak between 1 and 3 eV while a featureless shoulder centered at 0.7 eV seems to account for the two structures observed with high resolution at E_f and 280 meV. Even at 300 K the thermal broadening is negligible in comparison with the poor resolution of these data. The XPS spectrum (curve *A*) measured with a resolution of 300 meV locates already more correctly the center of gravity of the two low-energy peaks but does not separate them (see below).

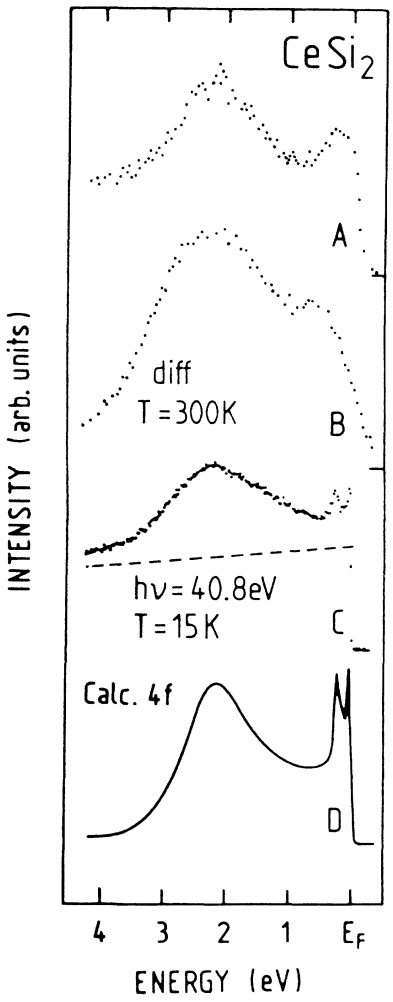

FIG. 12. Photoemission spectra of $CeSi_2$. *A*, room-temperature XPS measurement. *B*, $4f$-derived energy distribution curve measured with synchrotron radiation at 300 K (see text) (Ref. 15). *C*, spectrum recorded with a resolution of 40 meV at 15 K (Ref. 22). *D*, model calculation (NCA) of the $4f$ spectrum (Ref. 22).

In order to investigate the temperature dependence of the Kondo peak in $CeSi_2$, the $4f$ intensity has been extracted from the difference of high-resolution (18 meV) spectra excited with the He II and He I lines.[22] Curves (*a*)–(*d*) of Fig. 13 show the evolution of these *f* spectra between 15 and 300 K. In the measurement performed at 15 K, the temperature is substantially lower than the Kondo temperature $T_K = 35$ K so that the singlet ground state has the strongest weight in the initial state. The corresponding $4f$ spectrum (*a*) shows the two low-energy peaks already observed in γ-Ce (Fig. 10) but now much more pronounced. The spectral functions have been calculated taking into account finite temperatures and the crystal-field splitting.[22] For the lowest $f^1_{5/2}$ spin-orbit component, a CF splitting of 35 meV is assumed. The spectral function (*i*) calculated without instrumental broadening for 15 K shows that the lowest CF level gives rise to the important edge representing the true Kondo peak, followed immediately by a sharp peak accounting for the excited CF level. When the instrumental broadening of 18 meV is included, the spectral function (*e*) shows only a single peak at E_f with an apparent broadening of the edge, in perfect agreement with the measured spectrum (*a*). For increasing temperatures, the population of the singlet ground state is gradually weakened for the benefit of the nonsinglet magnetic states at higher energies. For $T > T_K$ the Kondo peak is washed

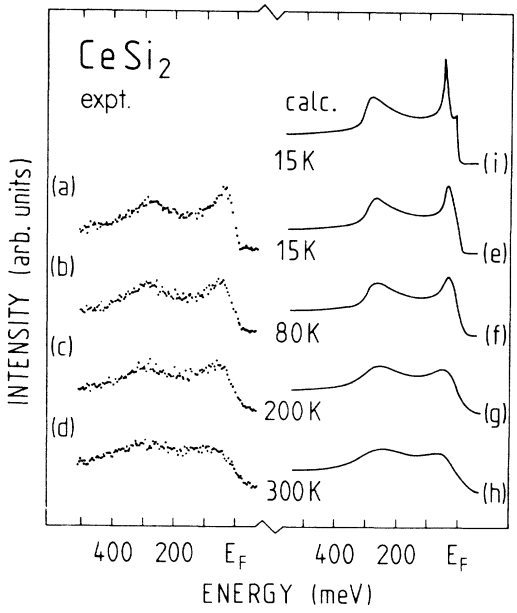

FIG. 13. Temperature dependence of the low-energy $4f$ excitations in the photoemission spectrum of $CeSi_2$ (Ref. 22). (*a*)–(*d*) experimental $4f$ contributions obtained from the difference of spectra recorded with the He II and He I lines. (*e*)–(*h*) model calculations (NCA) of the $4f$ intensity, including spin-orbit splitting, crystal-field splitting, influence of the temperature and instrumental broadening. (*i*) Same calculation as curve (*c*) but without instrumental broadening.

out and the $f^1_{7/2}$ peak broadens. In fact, the total $4f$ intensity in this 400 meV energy range is nearly temperature independent. A photoemission spectrum recorded with a resolution of a few tenths of an electron volt always shows a single peak at about E_F but does not reveal any indication of the high-temperature collapse of the Kondo peak.[12] In Fig. 12 this prediction is illustrated by the room-temperature spectra obtained by XPS (curve A) with a resolution of 300 meV[46] and by synchrotron radiation (curve B) with a resolution of 500 meV.[15]

D. The heavy-electron compound $CeCu_6$

Within the single-impurity model, a heavy-electron system is characterized by the fact that the hybridization strength is very weak in comparison to the energy separation of the two relevant $4f$ configurations ($4f^0$ and $4f^1$ in Ce). The weight n_f of the $4f$-symmetry states participating to the many-body ground state is nearly an integral number and is concentrated in the extremely narrow energy range δ. As a consequence, within δ the weight $n_f(1-n_f)$ of the photoemission signal reflecting directly this $4f$ admixture to the band becomes very weak.

The physical properties of $CeCu_6$ display the typical manifestations of heavy electrons.[4] As expected, the photoemission spectrum in the low-energy region shown in curve (a) of Fig. 14 contains a very weak $4f$ contribution.[17] The only characteristic feature which can be recognized is the tiny peak located at 280 meV above E_F. This observation reveals only indirectly the hybridization

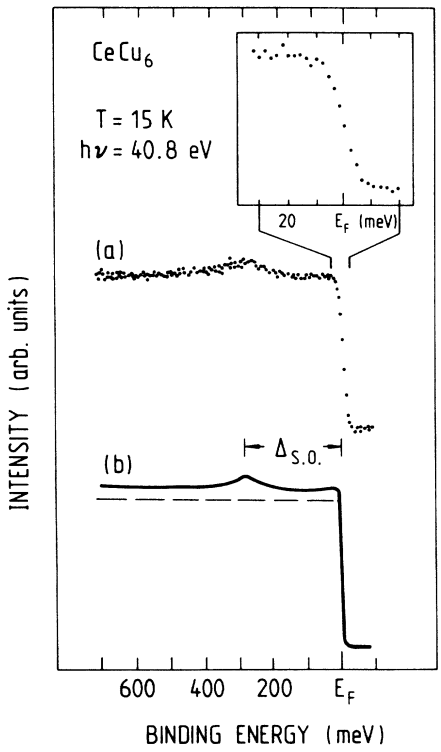

FIG. 14. Low-energy excitations in the photoemission spectrum of $CeCu_6$ (Ref. 17); (a) experimental spectrum measured with a resolution of 20 meV. (b) model calculation of the photoemission spectrum (GS). Inset: Fermi edge measured with a resolution of 12 meV.

since it corresponds to states of $4f^1_{7/2}$ character which are practically not involved in the initial state. However, this feature allows us to simulate the spectrum by a model calculation, as shown by curve (b) in Fig. 14. The dashed line representing the assumed band indicates that the $4f$ contribution is only a small fraction of the total intensity. From this analysis one obtains the value $\delta < 1$ meV corresponding to an integrated intensity of the Kondo peak $n_f(1-n_f) < 0.005$. This is too weak to be observed with the resolution of 20 meV achieved in the spectrum (a) and included in the calculation (6). As shown in the inset of Fig. 14, even with an improved resolution of 12 meV no indication of the Kondo peak can be discerned. These measurements have been performed at $T = 15$ K, a temperature somewhat higher than the Kondo temperature $T_K = \delta/k_B < 10$ K so that the Kondo peak may already be partly washed out by the thermal broadening (see preceding section).

E. $CeAl_2$—a frustrated heavy-electron compound

The compound $CeAl_2$ presents a very interesting situation, since only down to 10 K the specific-heat data can be interpreted within the single-impurity model including the crystal-field splitting of the $4f$ states.[50,51] At 4 K a transition occurs to an antiferromagnetic state with a reduced moment. The typical temperature dependence of the specific heat characterizing heavy-fermion systems cannot be observed at lower temperatures but an extrapolation from the higher temperatures yields a huge value of the order of 2000 mJ/mol K^2 for its linear coefficient $\gamma(T \to 0)$. The photoemission spectra B and C shown in Fig. 15 have been measured at 15 K.[19] For the photon energy $h\nu = 21.2$ eV, the $4f$ photoionization cross section is extremely small so that the spectrum B displays only the band states. For $h\nu = 40.8$ eV (spectrum C), the additional intensity accounting for the $4f$ emission is clearly recognized. It contains the characteristic $4f_{7/2}$ peak at 280 meV and at higher energies the broad structure of nearly pure $4f^0$ character, but here again no direct indication of the Kondo peak is observed. Curve C is the model calculation of this spectrum, including spin-orbit and crystal-field splittings. It yields the very small value $\delta = 0.2$ meV which is compatible with the analysis of the specific heat above the magnetic transition. This result demonstrates that even at a temperature above T_K, high-resolution photoemission spectra allow us to determine the single-impurity parameters. The necessity to obtain spectra of high quality is illustrated by curve A recorded at room temperature with synchrotron radiation. It is the $4f$-derived energy distribution curve obtained by the difference of on-resonance ($h\nu = 122$ eV) and off-resonance ($h\nu = 112$ eV) spectra.[52] A fair agreement with the high-resolution spectrum is found at energies higher than 1 eV but in the low-energy range near E_F, it fails completely to show the detailed structure which is the essential element of an accurate analysis. Furthermore, the difference technique used to derive curve A yields necessarily a distorted $4f$ intensity since the peaks near E_F and at about 2 eV are not resonating exactly at the same photon energy.[15]

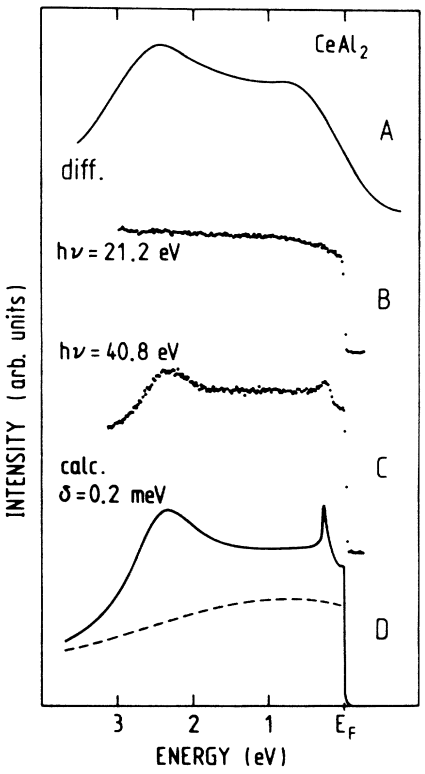

FIG. 15. Photoemission spectra of $CeAl_2$. *A*, $4f$-derived energy distribution curve measured with synchrotron radiation at 300 K (Ref. 52). *B* and *C*, spectra recorded with a resolution of 25 meV at 15 K (Ref. 19). *D*, model calculation (GS) of the high-resolution spectrum *C* (Ref. 19). The dashed line is the band used in the calculation.

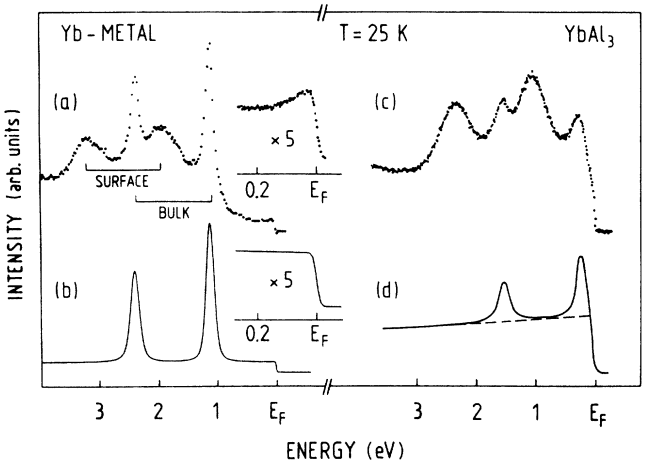

FIG. 16. (*a*) and (*c*) High-resolution photoemission spectra of Yb metal and $YbAl_3$ obtained with He II radiation in the full range of surface and bulk $4f$ excitations. (*b*) and (*d*) Model calculation (GS) simulating the bulk $4f$ contribution to the spectra (see text). The insets in (*a*) and (*b*) show the measured and calculated low-energy excitations for Yb metal, respectively (see text).

F. Yb metal—a mirror case to La metal

In heavy rare-earth systems, hybridization effects can also be important. For describing their f excitations one can take advantage of the mirror properties of an atomic shell with respect to its half population. The f spectra accounting for emission or addition of one electron can be exchanged between elements showing such a symmetry.[6] For example, the photoemission spectrum of divalent Yb metal with a $4f^{14}$ initial-state configuration corresponds to an inverse-photoemission spectrum of trivalent La with a $4f^0$ initial-state configuration. However, the $4f^{13}$ and $4f^1$ final states differ by the order and the binding energy of the $j=\frac{5}{2}$ and $\frac{7}{2}$ terms and by the magnitude of their splitting. Curve (*a*) of Fig. 16 shows the outer-level spectrum of an Yb-film evaporated and measured on a Cu substrate held at 25 K. The characteristic emission from bulk and surface $F^{13}_{7/2,5/2}$ multiplets is easily recognized.[53] Curve (*b*) of Fig. 16 displays the result of a single-impurity calculation for the bulk $4f$ photoemission obtained with the following parameters: $\varepsilon_f=1.08$ eV, $\Delta=50$ meV, and $\Delta_{s.o.}=1.27$ eV. The weak hybridization induces an energy lowering of the ground state $\delta=45$ meV and a not quite integral f population $n_f=13.98$ as in the case of La metal.[11] For this reason the experimental and calculated spectra show clearly that the tail of the less bound peak ($f^{13}_{7/2}$) is cut by E_F at a still sizable intensity so that the empty states contain a weak f contribution. A close inspection of the data in curve (*a*) of Fig. 16 (upper inset) reveals within the first 200 meV a peak culminating at E_F. This feature which is observed for the first time is incompatible with the f spectral function calculated within the single-impurity model (lower inset) and must be attributed to a structure of the band. In fact a band calculation of hcp Yb (Ref. 54) locates the Fermi level just at the onset of a very steep peak of the $5d$ band which is likely to explain the observed intensity increase in this narrow energy range.

G. $YbAl_3$—a mixed-valent compound

The alloy $YbAl_3$ displays many unconventional properties[55] reminiscent of those of Ce systems. This analogy originates most likely from similar hybridization mechanisms in both cases since the relevant f^{13} and f^{14} configurations of Yb and f^1 and f^0 of Ce have mirror properties as mentioned in the preceding section. Curve (*c*) of Fig. 16 shows a high-resolution (20 meV) uv spectrum of $YbAl_3$ measured at 25 K. The bulk $4f$ emission is recognized near E_F and at 1.5 eV, i.e., shifted by about 1 eV towards E_F when compared to Yb metal.[56] In Fig. 17 a more detailed high-resolution measurement of the low-energy region (spectrum *B*) is compared to an earlier photoemission spectrum of $YbAl_2$ measured with a resolution of 170 meV (spectrum *A*)[57] and to the single-impurity model calculation (curve *C*). For both compounds it appears clearly that the maximum of the peak, which has mainly $4f$ character, is not centered at E_F, but 240 meV above it. This observation is contradicting the intuitive model of valence fluctuation requiring the pinning of the lowest $4f$ excitation to E_F. This peculiarity

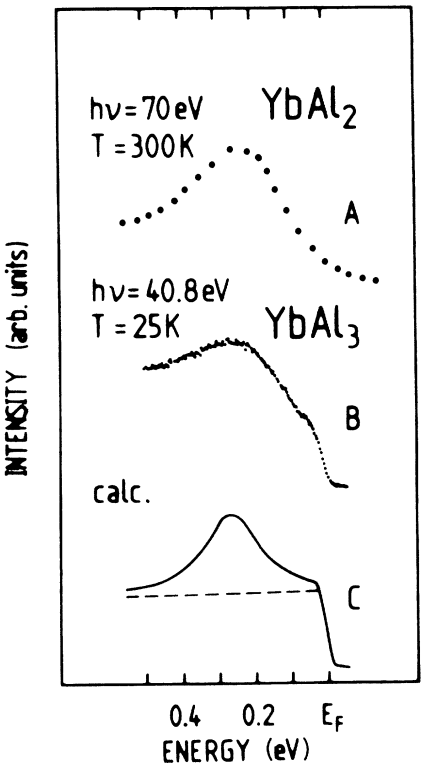

FIG. 17. Photoemission spectra of $YbAl_2$ and $YbAl_3$ in the low-energy range. *A*, spectrum measured with a resolution of 170 meV (after Ref. 57). *B*, spectrum measured with a resolution of 20 meV (Ref. 23). *C*, model calculation of the high-resolution photoemission spectrum (Ref. 23).

has been tentatively attributed to incomplete final-state screening and/or lattice relaxation effects.[57] The new aspect revealed by the high-resolution measurement and the model calculation is that this peak is extending up to the Fermi energy which cuts it. This means that such spectra do not account for the excitation of a localized $4f$ level which is broadened by a short lifetime and a poor instrumental resolution. It is a real continuum of $4f$ excitations. This fact is confirmed by the observation of the continuation of these excitations in the BIS spectrum[23,58] as a weak tail[59] which corresponds to the occupied Kondo peak in Ce systems. The very good simulation of the spectra by the model calculation yields a surprisingly large value $\delta=240$ meV corresponding in this case to the position of the peak maximum. This new situation results from the small-energy separation (0.2 eV) between the unhybridized f^{13} and f^{14} configurations and from the important hybridization strength ($\Delta=80$ meV). With $n_f=13.5$ it is a regime of intermediate valence which contrasts with the Kondo regime of Ce systems where n_f is always very close to an integral number. From measurements with conventional resolution it has also been concluded that $YbCu_2$ belongs to this intermediate valence regime.[60,61] The unexpected aspect of these results is that a hybridization strength comparable to those found in Ce is obtained in Yb. The mixing mechanism results from the overlap of the $4f$ wave functions of the rare-earth atoms with the wave functions of other symmetries belonging to neighbor atoms. From Ce to Yb, the extension of the $4f$ wave functions in the trivalent rare earths decreases by 30%.[12] One can anticipate a negligible $4f$ hybridization in Yb, in glaring contradiction with the previous analysis of the $YbAl_3$ spectra. In fact, starting from the trivalent state of Yb (f^{13}), the admixture of the $4f^{14}$ configuration increases the f count ($n_f=13.5$ in $YbAl_3$). The consequence is that the effective potential for $l=3$ is weakened so that the $4f$ wave-function tail is enhanced. In Ce the situation is reversed: the hybridization decreases the f count and localizes more strongly the $4f$ states. A simple theoretical estimation for realistic f counts shows that this mechanism can fully compensate the lanthanide contraction so that the same hybridization strengths can occur in Ce and Yb systems.[23]

VI. SPECTROSCOPIC DATA VERSUS GROUND-STATE MEASUREMENTS

In the preceding section we have presented and analyzed separately the spectra of different cerium and ytterbium systems covering a wide range of Kondo temperatures. It is now interesting to collect the single-impurity parameters deduced from these data and to test their compatibility with the experimental values of the zero-temperature susceptibility $\chi(0)$ and the linear coefficient $\gamma(T\rightarrow 0)$ of the specific heat which can also be calculated within the single-impurity model. In order to eliminate possible deviations originating from different numerical approaches, we have performed a new and unified analysis of all Ce systems with NCA. In an energy range of about 600 meV below E_F the f-excitation spectra have been extracted by subtracting from the He II spectra the He I spectra, after the normalization yielding the best elimination of the excitations reflecting states of other symmetries. From the top to the bottom of Fig. 18 [curves (a)–(f)], these data have been arranged in the order of decreasing hybridization strength. The NCA model calculations of these systems shown in the same order [(g)–(l)] have been performed at the temperatures of the experiments. They include spin-orbit and crystal-field splittings where appropriate. The instrumental resolution of 20 meV is taken into account by convoluting the calculated spectra with a Gaussian line of corresponding FWHM. With a suitable choice of the parameters, the model calculation yields a remarkably good simulation of the experimental spectra which have been normalized to the computed intensity. At this point, it would be extremely interesting to calculate $\gamma(T\rightarrow 0)$ and $\chi(0)$ within the NCA approach for the parameters deduced from the spectroscopic data, in order to test if the predicted values are consistent with those measured by these techniques. Unfortunately, we have encountered difficulties in the NCA calculations of these quantities, particularly for very heavy electrons. Already in the case of α-Ce which has the highest Kondo temperature among the systems we have investigated, this type of calculation predicts values larger than the experimental one by factors of 25 and 6 for $\gamma(T\rightarrow 0)$ and $\chi(0)$, respectively. For this reason we have used the values of δ and n_f deduced from our

spectroscopic data as input parameters in analytical expressions of these quantities. For the specific-heat coefficient we used the formula of Rajan[62] $\gamma(T\to 0)=N_A\pi k_B(N_f-1)/6T_0$, where the relation between the strong-coupling scale T_0 and the Kondo scale given by $T_0=T_k/1.29$ is only valid for $N_f=2$.[63] In all other cases we have set somewhat arbitrarily $T_0=T_K$. The expressions used for $\chi(0)$ are given in Sec. II A. [(Eq. (19) and following discussion]. Table I presents the single-impurity parameters obtained from our analysis, the values of $\gamma(T\to 0)$ and $\chi(0)$ calculated from these parameters, and the corresponding values measured in the direct experiments. Except for $YbAl_3$, the calculations predict systematically much larger values. At first sight this comparison is rather disappointing but is still worth some comments.

The linear coefficient of the specific heat represents certainly the quantity which has the closest relationship to the spectroscopic excitations. The measurement of $\gamma(T\to 0)$ is impeded in α-Ce by the difficulty to obtain a pure phase in bulk samples and in γ-Ce by the stabilization the high-temperature phase below the transition temperature. On the other hand, CeN is a peculiar compound, it has a very unstable stoichiometry and is likely to contain a very large nitrogen deficiency resulting in a strong decrease of the hybridization between f and band states.[18] In these three systems, important differences in the quality of the samples studied with the two methods may certainly be at the origin of large discrepancies between thermodynamic and spectroscopic values of $\gamma(T\to 0)$ but are unlikely to provide the complete explanation for the different orders of magnitude that we obtain. A possible explanation for this effect could lie in

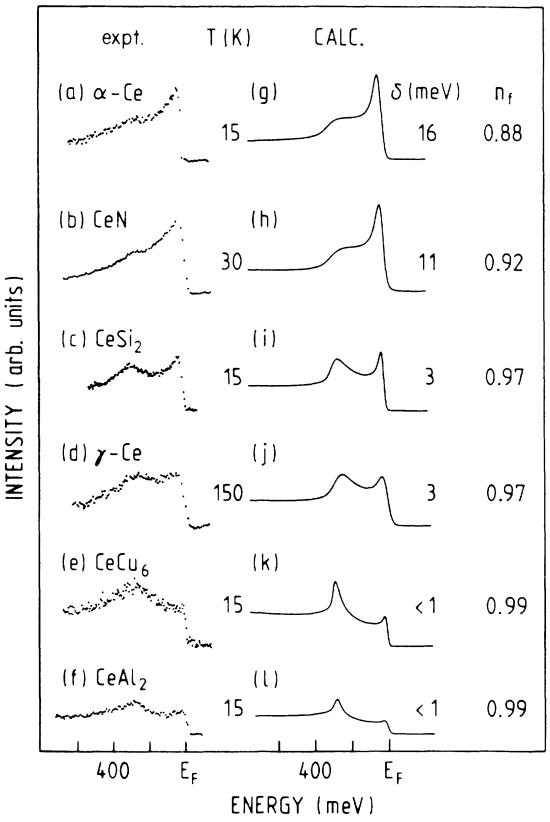

FIG. 18. Low-energy $4f$ excitations in the photoemission spectra of Ce systems. (a)–(f) Experimental contributions obtained by subtraction of He II and He I spectra measured with a resolution of 20 meV. (g)–(l) Model calculation of the photoemission spectra for the indicated temperatures (NCA).

TABLE I. Single-impurity parameters obtained from the analysis of our spectroscopic data in the different systems. The linear coefficient of the specific heat $\gamma(\to 0)$ and the magnetic susceptibility $\chi(T=0)$ are calculated with these parameters and compared with experimental values.

Material	Temperature (K)	n_f	δ (meV)	T_K (K)	N_f	$\gamma(T\to 0)$ (mJ/mol K^2) Calc.	Exp.	$\chi(T=0)$ (10^{-3} emu/mol) Calc.	Expt.
α-Ce	15	0.88	16	186	6	117	11.3[a]	3.8	0.66[a,k]
CeN	30	0.92	11	128	6	170	8.3[b]	5.8	2.9[b]
γ-Ce	150	0.97	3	35	6	622	7.5[c]		
$CeSi_2$	15	0.97	3	35	2	160	100[d,e]	5.17	4.2[e]
$CeCu_6$	15	>0.99	<1	<11.6	6	>1876	1600[f-h]	>68.8	17.7[f,g]
$CeAl_2$	15	>0.99	<1	<11.6	2	>375	135[i]	>15.8	50[j]
$YbAl_3$	15	13.5	240	2784	8	11	45[l]	0.46	4.62[m]

[a]Reference 64 (measured at a pression of 11 kbar).
[b]Reference 45.
[c]Reference 65.
[d]Reference 47.
[e]Reference 48.
[f]Reference 66.
[g]Reference 67.
[h]Reference 68.
[i]Reference 50 (1740, when extrapolated from the data above the antiferromagnetic transition).
[j]Reference 7.
[k]Reference 69.
[l]Reference 55.
[m]Reference 70.

the surface sensitivity of UPS. The number of nearest neighbors at the surface is reduced as compared to the bulk, leading to a hybridization weakening between $4f$ and band states.[18] The spectra would reflect this more localized situation and the extracted parameters would yield enhanced γ values. However, our XPS core-level spectra and UPS band spectra can be analyzed consistently with the same parameters. For the specific-heat measurements a correct extrapolation to $T=0$ is absolutely necessary. Very important errors in the determination of $\gamma(T\rightarrow 0)$ can result from a temperature range not extending to sufficiently low temperatures and where some discrete level is still weakly populated. In fact, with NCA we perform an analysis of photoemission spectra at the finite experimental temperature. However, if excited crystal-field levels at energies larger than δ and not resolved in our spectra are existing, the degeneracy $N_f=6$ should be reduced in our analysis and lower values of $\gamma(T\rightarrow 0)$ would be predicted. For the compounds $CeSi_2$, $CeCu_6$, and $CeAl_2$ the agreement between the measured and calculated values is satisfactory within the uncertainty resulting from our inadequate resolution for observing directly the Kondo peak in the very heavy-electron systems.

In the comparison of the $\chi(0)$ values also shown in Table I, the predictions based on the single-impurity parameters are again larger than the measured values. The previous arguments about samples and methods can also be invoked to explain these discrepancies. The situation is still more hazardous since the model is applied now to two rather different physical quantities. The case of $CeAl_2$ is particularly critical because this compound becomes antiferromagnetic below 4 K. A break in the general trend of the comparison presented in Table I is observed for $YbAl_3$. As discussed in Sec. V G, this compound is in an intermediate valence regime characterized by a very high T_K. In contrast to all Ce compounds, the calculated values of $\gamma(T\rightarrow 0)$ and $\chi(0)$ are smaller than those measured. It is too early to draw any conclusion from this single example but if this observation can be confirmed by further studies of Yb compounds, it would offer an interesting starting point to investigate the accuracy limits of the single impurity model when it is applied to extreme situations.

It seems very unlikely that the difficulties related to experimental techniques, data analysis, or sample quality can alone explain the discrepancies among the different values presented in Table I. The comparison of measured thermodynamic and spectroscopic data with the same quantities calculated using the Anderson Hamiltonian (H_A) calls for some general remarks concerning the role of the latter in the framework of many-body physics. H_A neglects all explicit electron-electron interactions except for the on-site Coulomb repulsion between f electrons. It is a simple but nontrivial approximation to the true many-body Hamiltonian H_{MB} of the system and it allows for a (more or less exact) explicit calculation of $\gamma(T\rightarrow 0)$, $\chi(T)$, and spectral functions by the use of techniques mentioned in Sec. II. The question that remains is how to link the values of the parameters appearing in H_A [see Eq. (1)] with some many-body calculations of the electronic structure of the solid. Various procedures have been proposed[71] using more or less convincing arguments for identifying these parameters with quantities showing up in band-structure calculations. However, considering H_A on more general grounds, as a trial Hamiltonian replacing H_{MB}, it is obvious that different optimization criteria can be applied—making, in each case, H_A the "best possible" trial Hamiltonian of the form given by Eq. (1)—depending on which physical observable should be evaluated by using H_A. Thus, quantities like n_f or δ may take different "optimal" values for thermodynamic functions and for photoemission spectra. We are currently developing such a trial Hamiltonian approach in order to find more precise relations between model parameters, like $V(\mathbf{k}m\sigma)$ and ε_f, and many-body expressions showing up, for example, in band-structure calculations.

The merit of this study is to show that the low-energy excitations related to the unconventional properties of heavy-fermion systems can be observed directly by high-resolution photoemission spectroscopy. Model calculations performed within the single-impurity model account remarkably well for their $4f$ spectra. The parameters extracted from this analysis are consistent with the trend that can be anticipated from their properties but when these values are used to calculate low-energy properties, in many cases they fail to predict the experimental data. These discrepancies raise the problem of the completeness of the single-impurity Hamiltonian for describing the different manifestations of heavy fermions. It would be extremely interesting to extend this type of study, at least its experimental part, to the more complex uranium systems showing heavy-fermion behaviors rather similar to those observed in rare-earth compounds.

ACKNOWLEDGMENTS

We acknowledge the Swiss National Science Foundation for financial support.

*Present address: Institut de Physique Expérimentale, Université de Lausanne, CH-1015 Lausanne, Switzerland.

[1]O. Madelung, *Introduction to Solid-State Theory,* Vol. II of *Springer Series in Solid-State Sciences* (Springer, Berlin, 1978), Chap. 1.

[2]G. Treglia, F. Ducastelle, and D. Spanjaard, J. Phys. (Paris) **41**, 281 (1980); Phys. Rev. B **21**, 3729 (1980), and references therein.

[3]F. Steglich, J. Aarts, C. D. Bredl, W. Lieke, D. Meschede, W. Franz, and H. Schäfer, Phys. Rev. Lett. **43**, 1892 (1979).

[4]G. R. Stewart, Rev. Mod. Phys. **56**, 755 (1984).

[5]O. Gunnarsson and K. Schönhammer, Phys. Rev. Lett. **50**, 604 (1983); Phys. Rev. B **28**, 4315 (1983); in *Handbook on the Physics and Chemistry of Rare Earths,* edited by K. A.

Gschneidner, L. Eyring, and S. Hüfner (North-Holland, Amsterdam, 1987), Vol. 10, Chap. 64.
[6]N. E. Bickers, D. L. Cox, and J. W. Wilkins, Phys. Rev. Lett. **54**, 230 (1985).
[7]P. A. Lee, T. M. Rice, J. W. Serene, L. J. Sham, and J. W. Wilkins, Comments Condens. Mater. Phys. **12**, 99 (1986).
[8]J. C. Fuggle, F. U. Hillebrecht, J.-M. Esteva, R. E. Karnatak, O. Gunnarsson, and K. Schönhammer, Phys. Rev. B **27**, 4637 (1983).
[9]J. C. Fuggle, F. U. Hillebrecht, Z. Zolnierek, R. Lässer, Ch. Freiburg, O. Gunnarsson, and K. Schönhammer, Phys. Rev. B **27**, 7330 (1983).
[10]F. U. Hillebrecht, J. C. Fuggle, G. A. Sawatzky, M. Campagna, O. Gunnarsson, and K. Schönhammer, Phys. Rev. B **30**, 1977 (1984).
[11]W.-D. Schneider, B. Delley, E. Wuilloud, J.-M. Imer, and Y. Baer, Phys. Rev. B **32**, 6819 (1985).
[12]Y. Baer and W.-D. Schneider, in *Handbook on the Physics and Chemistry of Rare Earths,* edited by K. A. Gschneidner, L. Eyring, and S. Hüfner (North-Holland, Amsterdam, 1987), Vol. 10, Chap. 62.
[13]J.-M. Imer and E. Wuilloud, Z. Phys. B **66**, 153 (1987).
[14]Y. Baer, J.-M. Imer. F. Patthey, and W.-D. Schneider, J. Electron Spectrosc. Relat. Phenom. **46**, 303 (1988).
[15]J. W. Allen, S. J. Oh, O. Gunnarsson, K. Schönhammer, M. B. Maple, M. S. Torikachvili, and I. Lindau, Adv. Phys. **35**, 275 (1986), and references therein.
[16]F. Patthey, B. Delley, W.-D. Schneider, and Y. Baer, Phys. Rev. Lett. **55**, 1518 (1985); **57**, 270 (1986); **58**, 1283 (1987).
[17]F. Patthey, W.-D. Schneider, Y. Baer, and B. Delley, Phys. Rev. B **34**, 2967 (1986).
[18]F. Patthey, S. Cattarinussi, W.-D. Schneider, Y. Baer, and B. Delley, Europhys. Lett. **2**, 883 (1986).
[19]F. Patthey, W.-D. Schneider, Y. Baer, and B. Delley, Phys. Rev. B **35**, 5903 (1987).
[20]Y. Baer, F. Patthey, W.-D. Schneider, and B. Delley, J. Magn. Mater. **63&64**, 503 (1987).
[21]W.-D. Schneider, F. Patthey, Y. Baer, and B. Delley, in *Giant Resonances in Atoms, Molecules and Solids,* Vol. 151 of *NATO Advanced Study Institute, Series B: Physics,* edited by J.-P. Connerade, J.-M. Esteva, and R. E. Karnatak (Plenum, New York, 1987), p. 461.
[22]F. Patthey, W.-D. Schneider, Y. Baer, and B. Delley, Phys. Rev. Lett. **58**, 2810 (1987).
[23]F. Patthey, J.-M. Imer, W.-D. Schneider, Y. Baer, B. Delley, and F. Hulliger, Phys. Rev. B **36**, 7697 (1987).
[24]W.-D. Schneider and Y. Baer, in *Narrow-Band Phenomena—Influence of Electrons with both Band and Localized Character,* Vol. 184 of *NATO Advanced Study Institute, Series B: Physics,* edited by J. C. Fuggle, G. A. Sawatzky, and J. W. Allen (Plenum, New York, 1988), p. 169.
[25]Y. Baer, F. Patthey, J.-M. Imer, W.-D. Schneider, and B. Delley, Phys. Scr. **T25**, 181 (1989).
[26]N. E. Bickers, D. L. Cox, and J. W. Wilkins, Phys. Rev. B **36**, 2036 (1987).
[27]N. E. Bickers, Rev. Mod. Phys. **59**, 845 (1987).
[28]T. V. Ramakrishnan, in *Valence Fluctuations in Solids,* edited by L. M. Falicov, W. Hanke, and M. B. Maple (North-Holland, Amsterdam, 1982), p. 13; P. W. Anderson, *ibid.* p. 451.
[29]Y. Kuramoto, Z. Phys. B **53**, 37 (1983).
[30]H. Keiter and G. Czycholl, J. Magn. Magn. Mater. **31**, 488 (1983).
[31]N. Grewe, Z. Phys. B **53**, 271 (1983).
[32]F. C. Zhang and T. K. Lee, Phys. Rev. B **28**, 33 (1983).
[33]P. Coleman, Phys. Rev. B **29**, 3035 (1984).
[34]H. Keiter and Q. Quin, Physica B+C **163B**, 594 (1990).
[35]E. Müller-Hartmann, Z. Phys. B **57**, 281 (1984).
[36]J. F. Herbst, R. E. Watson, and J. W. Wilkins, Phys. Rev. B **17**, 3089 (1978).
[37]J. F. Janak, Phys. Rev. B **18**, 7165 (1978).
[38]J. A. R. Samson, Rev. Sci. Instrum. **40**, 9 (1969).
[39]Y. Baer and Ch. Zürcher, Phys. Rev. Lett. **39**, 956 (1977).
[40]D. W. Lynch and J. H. Weaver, in Ref. 12, Chap. 66.
[41]D. M. Wieliczka, C. G. Olson, and D. W. Lynch, Phys. Rev. B **29**, 3028 (1984).
[42]J. W. Allen and R. M. Martin, Phys. Rev. Lett. **49**, 1106 (1982).
[43]E. Wuilloud, H. R. Moser, W.-D. Schneider, and Y. Baer, Phys. Rev. B **28**, 7354 (1983).
[44]R. Didchenko and F. P. Gortsema, J. Phys. Chem. Solids **24**, 863 (1963).
[45]J. Danan, C. de Novion, and R. Lallement, Solid State Commun. **7**, 1103 (1969).
[46]E. Wuilloud, B. Delley, W.-D. Schneider, and Y. Baer, J. Magn. Magn. Mater. **47&48**, 197 (1985).
[47]W. H. Dijkman, A. C. Moleman, E. Kesseler, F. R. deBoer, and P. F. de Châtel, in *Valence Instabilities,* edited by P. Wachter and H. Boppart (North-Holland, Amsterdam, 1982), p. 515.
[48]H. Yashima and T. Satoh, Solid State Commun. **41**, 723 (1982).
[49]H. Yashima, H. Mori, T. Satoh, and K. Kohn, Solid State Commun. **43**, 193 (1982).
[50]C. D. Bredl, F. Steglich, and K. D. Schotte, Z. Phys. B **29**, 327 (1978).
[51]B. Coqblin, A. K. Bhattacharjee, R. Jullien, and J. Flouquet, J. Phys. (Paris) Colloq. **41**, C5-297 (1980).
[52]R. D. Parks, S. Raaen, M. L. deBoer, Y.-S. Chang, and G. P. Williams, J. Magn. Magn. Mater. **47&48**, 163 (1985).
[53]W.-D. Schneider, C. Laubschat, and B. Reihl, Phys. Rev. B **27**, 6538 (1983).
[54]O. Jepson and O. K. Anderson, Solid State Commun. **9**, 1763 (1971).
[55]E. E. Havinga, K. H. J. Buschow, and H. J. Van Daal, Solid State Commun. **13**, 621 (1973).
[56]B. Johansson and N. Mårtensson, in Ref. 12, Chap. 69.
[57]G. Kaindl, B. Reihl, D. E. Eastmann, N. Mårtensson, B. Barbara, T. Penny, and T. S. Plaskett, Solid State Commun. **41**, 157 (1982).
[58]S.-J. Oh, S. Suga, A. Kakizaki, M. Taniguchi, T. Ishii, J.-S. Kang, J. W. Allen, O. Gunnarsson, N. E. Christensen, A. Fujimori, T. Suzuki, T. Kasuya, T. Miyahara, H. Kato, K. Schönhammer, M. S. Torikachvili, and M. B. Maple, Phys. Rev. B **37**, 2861 (1988).
[59]Our results differ from those of Ref. 58. It seems that there exists a problem of sample stability because fractured samples sometimes yielded similar spectra as obtained from our scraped samples [J. W. Allen (private communication)]. The main point of interest of the present study is, however, the single-impurity behavior of the Yb ions, which is clearly demonstrated by our experimental results and their analysis.
[60]A. Fujimori, T. Shimizu, and H. Yasuoka, Phys. Rev. B **35**, 8945 (1987).
[61]Y.-S. Huang and V. Murgai, Solid State Commun. **69**, 873 (1989).
[62]T. V. Rajan, Phys. Rev. Lett. **51**, 308 (1983).
[63]N. Andrei and J. H. Löwenstein, Phys. Rev. Lett. **46**, 356

(1981).
[64]N. E. Phillips *et al.*, Phys. Lett. A **27**, 49 (1968).
[65]D. C. Koskenmaki and K. A. Gschneidner Jr., in Ref. 12, Vol. 1, p. 337.
[66]Y. Onuki *et al.*, J. Phys. Soc. Jpn. **53**, 1210 (1984).
[67]G. R. Stewart *et al.*, Phys. Rev. B **30**, 482 (1984).
[68]H. R. Ott *et al.*, Solid State Commun. **53**, 235 (1985).
[69]A. J. T. Grimberg *et al.*, Solid State Commun. **11**, 1579 (1972).
[70]J. C. P. Klaase *et al.*, Physica B+C **106B**, 178 (1981).
[71]See eg. O. Gunnarsson, O. K. Andersen, O. Jepsen, and J. Zaanen, Phys. Rev. B **39**, 1708 (1989), and references therein.